ELSEVIER

Contents lists available at ScienceDirect

Journal of Power Sources

journal homepage: www.elsevier.com/locate/jpowsour





X-ray photoelectron spectroscopy as a probe for understanding the potential-dependent impact of fluoroethylene carbonate on the solid electrolyte interface formation in Na/Cu₂Sb batteries

Nathan J. Gimble ^a, Leslie A. Kraynak ^a, Jacob D. Schneider ^a, Maxwell C. Schulze ^b, Amy L. Prieto ^{a, *}

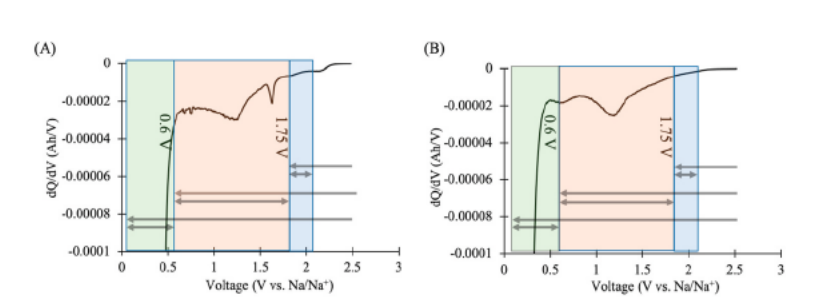
HIGHLIGHTS

- First use of XPS on binder-free copper antimonide anodes to assess SEI formation.
- Use of differential capacity to identify SEI growth in distinct voltage regions.
- Unique XPS methodology to identify SEI heterogeneity.
- Analysis of the effect of FEC on the SEI formed on the active material.
- Elucidation of the effect of FEC on inhibiting SEI formation at different voltages.

ARTICLE INFO

Keywords: Batteries Sodium Additives Electrolyte XPS

GRAPHICAL ABSTRACT



ABSTRACT

The solid electrolyte interface (SEI) forms from electrolyte decomposition during the initial discharge of half-cell batteries and is affected by the presence of electrolyte additives. Breaking down the initial discharge into stages, defined by voltage cut offs, can help discover the role of additives in SEI growth. In this study, X-Ray Photoelectron Spectroscopy (XPS) is used to analyze the SEI formed on electrodeposited, binder free Cu₂Sb thin films in sodium ion half-cell batteries. The presence of fluoro-ethylene carbonate (FEC), an electrolyte additive known to enhance battery lifetime, has a significant effect on the carbon 1s XPS spectra. The concentration of oxygenated carbon environments are dramatically decreased when FEC is added to the system. These environments were present in samples without FEC before significant electrochemistry was observed, potentially displaying the reactivity of sodium metal with conventional carbonate electrolytes to form the initial components of the SEI before the battery is cycled. The differences observed when FEC is added are likely the chemical environments of the SEI that have the dramatic effect on battery performance. Interestingly, these results suggest that the critical aspects of SEI formation are determined before the active material is sodiated, with FEC playing an integral role.

E-mail address: alprieto@colostate.edu (A.L. Prieto).

a Department of Chemistry, Colorado State University, Fort Collins, CO, 80523, USA

b National Renewable Energy Lab, Golden, CO, USA

^{*} Corresponding author.

1. Introduction

Energy storage is a critically important area of research due to the emergence of the lithium ion battery (LIB), which has led to the proliferation of portable electronic devices and fully electric vehicles. High capacity batteries have broader applications with the threat of climate change requiring the development of renewable energy sources in parallel with energy storage technologies [1]. There are concerns about the availability of lithium in terms of the scaling of battery technology to large-scale grid storage applications. Sodium ion batteries (NIB) cost 30% less compared to LIBs and sodium is three orders of magnitude more abundant in the earth's crust, making it a target for large-scale energy storage applications [2].

Current commercial LIBs and developing NIBs use an organic liquid electrolyte to facilitate the diffusion of the working ion between the electrodes [3]. The electrochemical window of these electrolytes is within the operating voltage of the battery, degrading the electrolyte to pseudo-passivate the anode surface forming the solid electrolyte inter face (SEI) [3-5]. The electrolyte solvent used ubiquitously in battery literature and commercial battery construction is comprised of different organic carbonates including ethylene carbonate (EC) and propylene carbonate (PC) usually mixed with dimethyl carbonate (DMC) and diethyl carbonate (DEC) [3,6-9]. There are numerous variations on this theme adding to the complexity of the literature as each electrolyte component contributes to the SEI's composition and properties [6,10]. The supporting electrolyte also plays a role in SEI formation adding another layer of variability. Lithium hexafluorophosphate (LiPF 6) is the most common supporting electrolyte; lithium perchlorate (LiClO 4), lithium bis(trifluoromethane) sulfonimide (LiTFSI), lithium bis(oxalate) borate (LiBOB), as well as more toxic salts are present in the literature as well [6,10,11]. These same anions and electrolyte solvents have been used to study analogous sodium ion battery systems [12-14].

The SEI is extremely important in battery performance, requiring specific properties: it should be electronically insulating to prevent additional electrochemical reduction of the electrolyte, ionically conductive to allow the supporting ions to travel through to the electrode surface, and mechanically stable as to not expose new surfaces for additional SEI formation [15–19]. Between the first and second cycle of a LIB or NIB, there is a large irreversible capacity loss sometimes as great as 60% attributed to SEI formation [20]. During SEI formation, the properties described are self-selected for by the conditions in which the SEI is grown. Additionally, the SEI is a failure mechanism as uncon trolled SEI growth over subsequent cycles exacerbates pulverization of the anode or completely impedes ionic mobility [5,21,22]. The SEI functions as a solid electrolyte, thus studying its components has applications beyond batteries, potentially also enabling the progress of discovering fast ion conductors.

Specific small molecule additives have been used widely in battery literature to improve battery performance [6,10,23,24]. Fluoro-ethylene carbonate (FEC), one such additive, has been widely used to extend battery lifetime [25-29]. Previous modeling and experimental research on FEC found it to act sacrificially forming preliminary SEI components to control growth [30-38]. One hypothesis explaining the beneficial properties of FEC is that it assists with ion conduction in the SEI by creating nano-scale deposits of LiF, or NaF in the sodium analog, while creating an electronically insulating surface [25]. However, this hypothesis is not known conclusively. The same idea applies to the utilization of LiPF₆, which also adds fluorine to the system [11,39]. While trends are emerging regarding the role of additives, further characterization of the SEI species on the surface is required to link structure to properties. Additives used in Li-ion systems have been used in Na-ion batteries showing improved battery performance, which is unprecedented [12-14]. Further research is needed to learn more about how the small additives such as FEC form the SEI in a sodium system to guide optimization and development.

In order to further improve liquid electrolytes, especially for Na-ion

batteries, a thorough understanding of what components are present on the anode surface at a particular voltage in the cycling process, especially with regards to the effect of additives is crucial [40]. Without exploring this issue more, it is difficult to understand how the SEI is functioning. Through experimentation in a lithium system, the SEI is thought to contain organic and inorganic components that may or may not be formed in layers [41,42]. Reaction schemes and models have been proposed to describe electrolyte decomposition, however, the products shown in these reactions do not provide a complete under standing of the SEI's effect on battery performance as it is difficult to relate these results back to the desired SEI properties [16,30,31,43-45]. The majority of studies performed on the SEI use a lithium ion system, which cannot always be directly applied to sodium. Lithium and sodium have different reactivities, alloying pathways, and migration properties; understanding how these differences apply to SEI formation will lead to important information about ionic conductivity, electrolyte selection and reactivity [46,47]. Recent studies have been exploring the differ ence in sodium and lithium reactivity revealing sodium metal to be spontaneously reactive with carbonate electrolytes making it a lower quality reference and counter electrode for half-cell battery experiments [48–54]. The role of FEC in this reactivity is particularly interesting as recent work from Dugas et al., 2016 proposes that FEC forms a protec tive layer on the surface of Na metal that assists with battery cycling [49]. Understanding this reactivity and what role it plays in the growth of the SEI on pure phase active material will be critical for improving and optimizing NIB systems for researching novel electrode materials.

Measuring and understanding how, as well as if, the SEI forms at different points during battery cycling is a difficult task. Differential capacity analysis takes the differential of the total charge passed as a function of voltage. Peaks in differential capacity are a sign of an elec trochemical event at a particular voltage and may be used to observe when SEI is forming on the working electrode. However, because the SEI forms under anerobic conditions as a thin film on the surface of the anode material, it is not trivial to accurately determine what has formed. Many analytical techniques have been used to characterize the SEI however, no single technique is capable of elucidating its true nature as once again it is difficult to correlate results to the desired SEI properties [19,55]. X-ray photoelectron spectroscopy (XPS) is the most applicable technique used to study SEI as it is surface sensitive and will be the primary tool used in this study [15,19]. XPS is minimally invasive however, remaining cognizant of how utilizing a specific analytical technique is changing the SEI is important [56]. Because many of the applicable techniques are performed ex-situ, the operation of disassembling the battery in and of itself may be changing the SEI in some capacity [57]. In XPS interpretation, no conclusion will be made that reaches beyond the capability of the technique.

The previous work studying SEI is inconsistent as variables tested such as lithium vs. sodium, electrolyte composition, cycle rate, voltage ranges, and electrode material are often not taken into account [15,18, 19]. Additionally, the heterogeneity of SEI species is not heavily researched, an important note as anode materials and substrate prop erties may play a role in SEI growth. Fabrication of anode materials commonly utilizes carbon binders, convoluting whether the carbon signal is from the binders or the SEI in the carbon XPS and introducing reactive surface sites for SEI growth. Additionally, the presence of binders fundamentally changes the chemical properties of the surface which can change how SEI grows [58]. The SEI forms from the elec trolyte primarily during the initial charge, or discharge in the case of half cells, and it is likely at this stage that the crucial aspects of the SEI are forming that affect battery lifetime. Preceding studies have tried to break apart the initial cycle based on Li/Na alloying rather than po tentials corresponding to SEI formation leading to results that do not represent how the SEI is growing [59-63].

In this study, XPS is used to analyze electrodeposited Cu $_2$ Sb as an anode material assembled in a sodium ion battery half-cell. The anode Cu $_2$ Sb was chosen as it is a promising anode material due to it

cyclability, high electrical and thermal conductivity, and resistance to pulverization [64,65]. Electrodeposited Cu ₂Sb provides a unique system to study how SEI forms on pure high density alloys without the presence of binders. We study conventional electrolytes with and without FEC to elucidate the additive's role in SEI growth. To examine SEI growth, the initial discharge of the half-cells were broken into regions based upon features in the differential capacity to discover a correlation between electrochemical events and XPS elemental environments. This hypoth esis leads to understanding at what point crucial SEI components are being formed and focus on the particular chemical reactions occurring can begin. Sodium perchlorate was the supporting electrolyte assuring that FEC is the sole fluorine source in the system. The additive FEC was found to have a significant effect on the carbon XPS signals suppressing the singly oxygenated and carbonate carbon environments from the very beginning of battery cycling. This signifies that FEC plays an immediate role in which components are present on the surface of the anode ma terial. This leads to the understanding of how these components contribute to the desired SEI properties.

2. Experimental

2.1. Electrodeposition of the C₂Sb electrode

The Cu₂Sb anode material being studied was synthesized via electrodeposition. The electrodeposition solution was comprised of 400 mM citric acid and 25 mM antimony(III) oxide (Sb 2O3, nanopowder, 99.9+ % Aldrich) which was left to dissolve with the help of mechanical stirring for 12 h at 60 °C. When the solution was clear, 80 mM copper(II) nitrate hemipentahydrate (Cu(NO₃)₂, 99.9+ % Aldrich) was added turning it to a vibrant light blue. This solution was then titrated dropwise, with continued mechanical stirring, to pH 6 with saturated KOH, causing the color to shift to a darker royal blue. All water used in the electrodepo sition solution was Millipore water (18 $M\Omega$). Copper substrates were prepared by electropolishing for 15 s in a solution of 2:1 H ₃PO₄: H₂O to remove the oxide layer on the copper surface. The substrate was thor oughly washed with Millipore water, rinsed with 200 proof ethanol, and air dried. A custom electrodeposition cell (SI Figure S1) was used where the substrate was the working electrode with a stainless-steel mesh as the counter electrode and a saturated calomel electrode (SCE) as the reference electrode. A Gamry Reference 3000 potentiostat was used to apply a constant voltage of 1.05 V vs. SCE for 10 min to form the purple-grey pure phase copper antimonide anode material, which was used to study SEI formation. This copper antimonide synthesis was developed and discussed in a previous report [66].

2.2. Battery assembly and cycling

Half-cell batteries were assembled in an argon glove box (O 2 < 1 ppm) using Swagelok PFA straight tube fittings with a half-inch bored center. Half-inch punches from Cu 2Sb films, Na metal, two polypropylene (PP) separator punches, glass microfiber filter paper (Whatman), 200 mL of electrolyte solution, and stainless steel mesh were assembled in the configuration shown in SI Figure S2. The electrolyte solution comprised of 1 M sodium perchlorate (NaClO 4, Sigma Aldrich ACS Reagent) supporting electrolyte dissolved in 1:1:1 portions of ethylene carbonate (EC, recrystallized), dimethyl carbonate (DMC, Anhydrous Sigma Aldrich ≥99%), and diethyl carbonate (DEC, Sigma Aldrich Anhydrous 99%) by weight, as well as for certain experiments, 5% fluoroethylene carbonate (FEC, Sigma Aldrich ≥99%) by volume. The half cells were cycled on an Arbin BT2000 series battery tester under constant current conditions. Preliminary half cells were subjected to 5 discharge and charge cycles between 2 and 0.02 V vs. Na/Na at a rate of C/50. Subsequent potential region experiments were cycled between 2 and 1.75 V, 1.75 and 0.6 V, and finally 0.6 and 0.02 V vs. Na/Na $^+$ for the high (HPR), middle (MPR), and low (LPR) potential regions respectively. Each battery potential region cycling experiment was

repeated four times with Cu₂Sb punches from four different electrodeposited films. These regions were used for samples with and without FEC. It should be noted that three additional experiment repetitions were performed for the LPR batteries without FEC, and all were consistent with each other. Potential regions experiments were cycled twenty times across their respective voltages. Twenty cycles is sufficient time at these potential regions to develop any electrochemical products on the anode surface for analysis. Figure S3. Depicts capacity vs. cycle number for each potential region experiment. Cycled cells were dis assembled in the argon glovebox and the Cu₂Sb films were washed with 300 µL of DMC before transfer to the X-ray photoelectron spectrometer (XPS) using a sealed air-free transfer holder. Each potential region had many replicate samples to get an idea of heterogeneity in each sample and reproducibility.

2.3. X-ray photoelectron spectroscopy

Samples were transferred air-free from the argon glove box to the PE-5800 series Multi-Technique ESCA system intro chamber where 30 min high resolution (HRES) scans were performed on two center spots and one edge spot for each anode. Examining multiple spots will explore heterogeneity across a single SEI surface. Additionally each experiment was repeated four times using different electrodeposited films to explore the reproducibility of SEI formation. An Al K α monochromatic source operating at 350.0 W is used for all XPS experiments. High resolution scans were used to analyze all possible elements: carbon 1s, oxygen 1s, chlorine 2p (SI Figure S6), fluorine 1s, and sodium 1s. For the high potential region, copper 2p and antimony 3d were also detected. A selfconsistent fitting method using CasaXPS software was employed to analyze the results. All high-resolution spectra were calibrated to the aliphatic carbon peak at 285 eV. This calibration method uses the assumption that lowest binding energy carbon peak is aliphatic carbon in the sample and is a common XPS fitting practice [67,68]. Other peaks in the system matched appropriately making the calibration self-consistent. That being said, comparing peak position to other work may not be appropriate as a different instrument and battery assembly conditions may result in a different aliphatic carbon calibration. The fitting process utilizes a Shirley background to account for when the background shifts at higher binding energies. Peaks were fit using an Ockham's Razor-style approach looking to minimize the number of binding environments that were used to match the data. All fitted peaks are gaussian and for a given element the full width half max (FWHM) is constrained to not exceed 1.5 times any other peak as it is unlikely that environments from the same element have highly variable FWHM. Photoelectrons with split peaks such as the chlorine 2p and antimony 3d are constrained to each other completely following the known infor mation about each split [69]. Finally, the percent composition of each element and chemical environments was calculated by Casa XPS using relative sensitivity factors (RSF) values from Physical Electronics [69].

2.4. Data analysis

Each element's raw XPS spectra from replicate samples were overlaid and an average spectra was created to show heterogeneity. Creating an average spectra required first subtracting the variable baseline counts of each spectra due to inconsistent chamber pressure. A Python code was written that subtracted every Y electron counts/second value by the smallest measured number in a particular scan, which was used as the baseline value. After the transformation, overlaid spectra could be compared visually and an average spectra could be created. The code created the average spectra by binning each X-axis binding energy value to the nearest 0.1 eV then averaging each corresponding Y-value across every replicate scan. This creates an average spectrum for each element in each potential region in an attempt to account for heterogeneity. The Python code used in the baseline subtraction and spectra averaging can be found in the supporting information. The development of an average

spectrum allows for trends in each region to be observed more clearly. Quantification data derived from fit peaks, which was unaffected by the background subtraction as it was already based upon peak area above the background, was used to understand the differences in SEI samples and compare replicate samples. The peak position and environment concentration for each fitted peak in replicate samples was averaged giving a standard deviation, effectively representing the amount of heterogeneity for that environment in a given set of samples. An example of the Python code used is in the SI figure S4.

3. Results and discussion

In order to explore the electrochemistry of the initial discharge for this system, a battery with and without FEC was cycled at a C/50 rate.

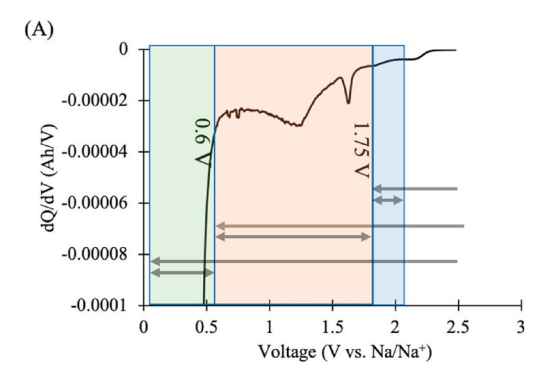
Differential capacity plots of the batteries cycled at the slow rate (C/ 50) were used to formulate three potential regions in the initial discharge of the half-cell battery as shown in Fig. 1. The first region between 2 and 1.75 V vs. Na/Na, and finally, herein defined as the high potential region (HPR), is where very little if any electrochemistry is occurring. The middle potential region between 1.75 and 0.6 V vs. Na/ Na⁺ (MPR) is where electrolyte decomposition electrochemistry is occurring but no reductive sodiation of Cu 2Sb. Both experiments with and without FEC have peaks centered at 1.25 V vs. Na/Na contained in this region. Sodiation electrochemistry is contained in the low potential region (LPR) between 0.6 and 0.02 V vs. Na/Na, the onset of the sodiation event is observed occurring at 0.5 V vs. Na/Na⁺. There was no significant difference in these voltage regions when FEC was added, thus to keep this variable consistent, the selected regions were used for both sets of experiments. XPS can be used to explore any correlation between the electrochemistry observed in differential capacity to the different species on the surface of CbSb.

Differential capacity plots for HPR samples, MPR samples and LPR samples cycled with 1:1:1 EC:DMC:DEC electrolyte solvent with and without FEC are shown in Fig. 2. Generally, the electrochemistry observed in replicate experiments for each potential region were similar with the most significant differences occurring in the MPR. However, these differences are minute, as the Ah/V values are very small. The differences observed are likely due to variable surface roughness, local Cu-Sb ratios and amorphous oxides present [70]. The Y-axis of the HPR differential capacity plots are an order of magnitude smaller than the middle and low potential regions confirming little to no electrochem istry is occurring in the selected voltage region. The onset of electrolyte reduction occurring in the MPR as seen as larger differential capacity values are approximately two times larger for samples without FEC. This is counterintuitive as FEC is thought to act sacrificially during the initial SEI growth [30-37]. The LPR differential capacity plots reflect this phenomenon as well showing more capacity passed in samples without FEC before the reductive sodiation of Cu₂Sb. Lower charge passed

suggests that the presence of FEC impedes the amount of electrolyte reduction in the initial discharge potentially resulting in a longer battery lifetime. Monitoring differential capacity ensured that each battery had similar electrochemical events occurring on the Cu_2Sb surface matching the original goal of identifying SEI growth based on electrochemistry observed.

High resolution carbon 1s XPS spectra from CbSb samples cycled in the different potential regions with and without FEC are shown in Fig. 3. The quantification of fitted peaks are presented in Fig. 4, numerical quantification values for this plot are present in SI Table S1. In addition, the average peak position for each fitted peak is tabulated in the SI. It should be noted that the standard deviation of the average peak position ranged from 0.02 to 0.6 eV. This implies that in replicate samples, heterogeneity is based not on the components changing but rather their relative abundances. There are four carbon environments of various levels of oxidation. The first fitted peak is aliphatic carbon at 285 eV, which is present in all spectra collected. Aliphatic carbon is present in the majority of XPS as most surfaces exposed to atmosphere gather it on the surface. This makes it difficult to determine how much C-C and C-H environments are coming from SEI and how much is adventitious. especially since adventitious carbon is not controlled [67]. In experi ments cycled in the MPR and LPR without FEC, the aliphatic peak has significant error likely due to variable adventitious carbon. Singly oxygenated carbon, also present in every sample, appears at 286.8 eV. At 288.6 eV is the carboxyl carbon environment appearing in a consistent, small concentration across each sample with slightly higher average concentrations in FEC-containing experiments. Finally the carbonate environment appears at 290 eV without FEC and 291 eV with FEC. The carbonate environment is not present in the HPR FEC containing bat teries but appears in the MPR and persists in the LPR. XPS spectra are taken under ultra-high vacuum, thus these carbon environments are representative of SEI species adhered onto the surface and not any residual electrolyte.

The striking difference in these sets of carbon XPS spectra is the significantly larger singly-oxygenated and carbonate carbon environment in the HPR samples without FEC compared to samples with FEC. The concentration, as calculated from the fitting of peak areas, of these peaks is nearly *double* when FEC is not present. Since these carbon environments have appeared on the C½Sb anode surface in the HPR where the electrode is only slightly polarized, they form before significant electrochemistry has occurred. Measuring SEI species in the HPR contradicts the original hypothesis that electrochemistry observed in the differential capacity plots could be correlated to SEI growth. Instead, the presence of these carbon environments implies that in the HPR, the SEI is forming spontaneously on the active material before any current is applied. Previous research into spontaneous reactivity of sodium metal have only examined the effect on the sodium counter electrode or comparing half-cells to full cells but not on the anode material [51].



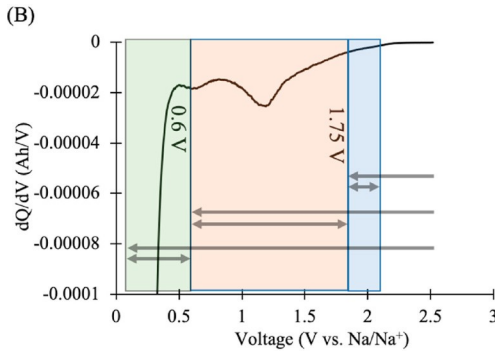


fig. 1. Differential capacity plot of the first discharge for sodium ion batteries with a A) 1 M NaClO 4 1:1:1 EC:DMC:DEC and B)+ 5% FEC. Highlighted potential regions are shown in blue, orange and green for the HPR, MPR, and LPR respectively where batteries were cycled 20 times. (For interpretation of the references to color in this figure legend, the reader is referred to the Web version of this article.)

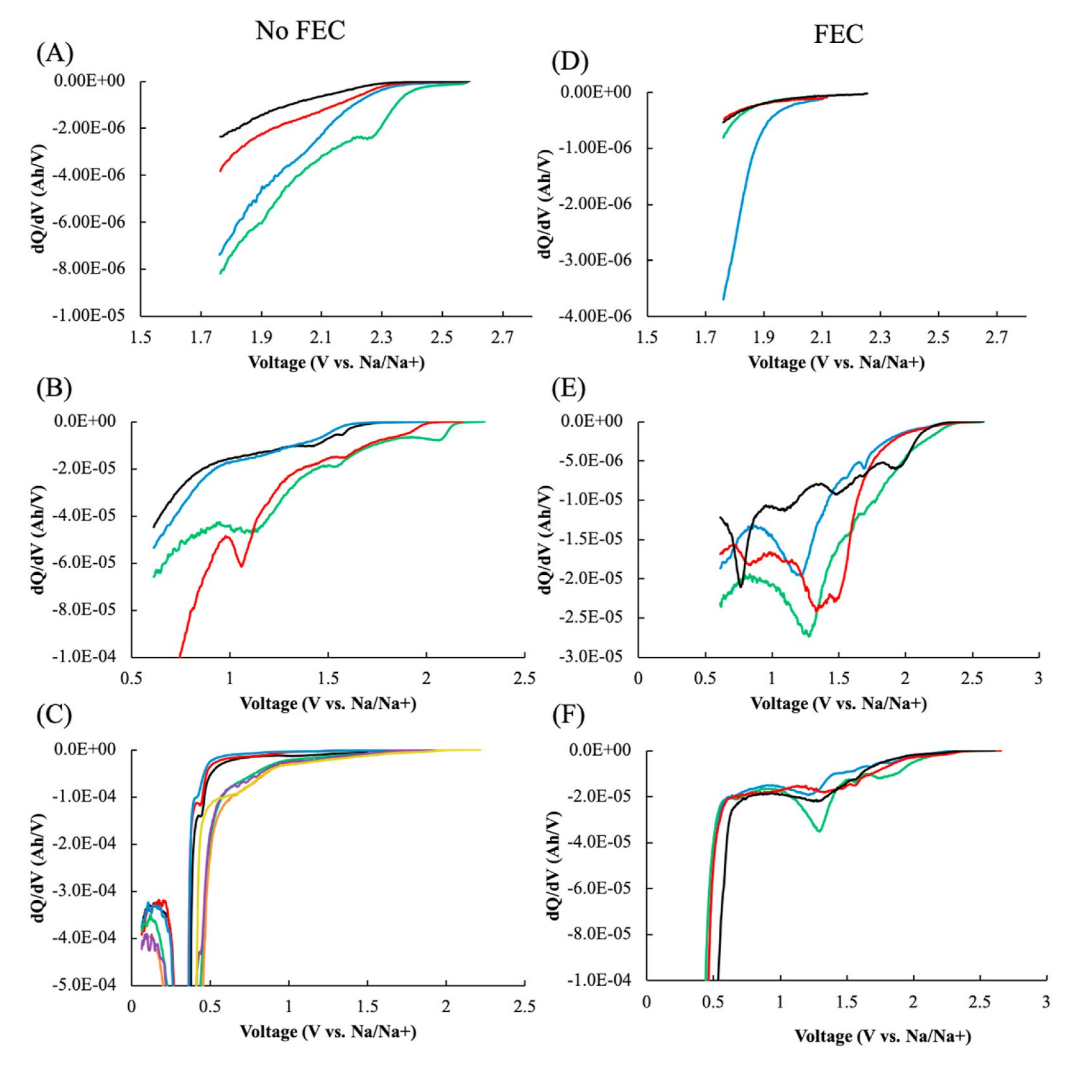


fig. 2. Differential capacity plots for replicate battery samples cycled with 1 M NaClO 4 1:1:1 EC:DMC:DEC in the A) HPR, B) MPR, and C) LPR, then batteries with 5% FEC vol. cycled in the D) HPR, E) MPR, and F) LPR.

Ultimately, the singly oxygenated and carbonate environments observed in the HPR suggest that sodium metal reactivity affects SEI formation in half-cells before electrochemistry has occurred. Moreover, when FEC is incorporated in the electrolyte, the HPR samples have minimal carbon environments associated with electrolyte reduction (adventitious car - bon is still present) on the surface. This suggests that FEC may be preventing sodium metal from reacting with the electrolyte and depositing reaction products onto the active material's surface as initial SEI com - ponents which is different from what is hypothesized to occur in lithium systems. Exploring this reactivity and its effect on SEI growth is the focus of ongoing research.

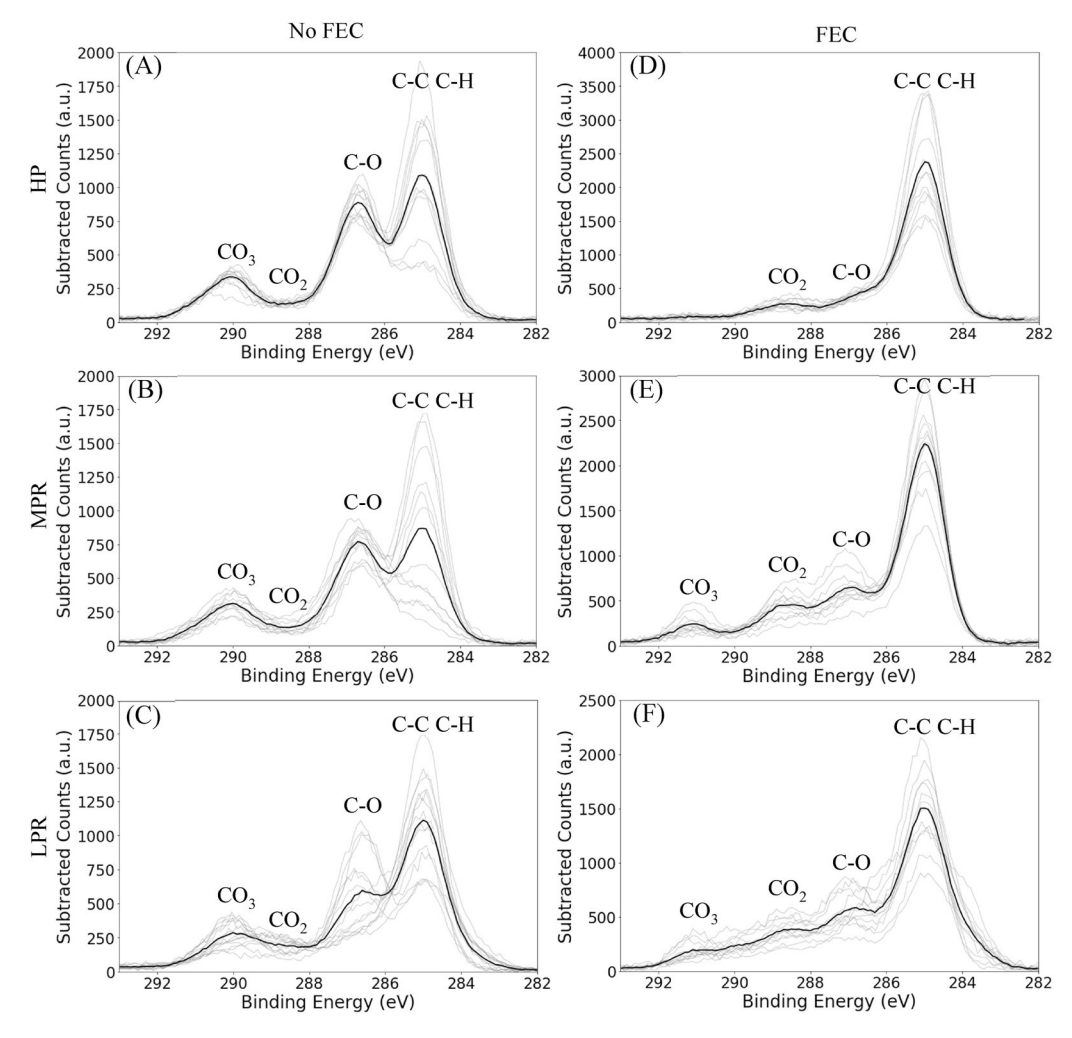
When more reductive current is passed in the MPR, a carbonate carbon peak at 291 eV emerges as well as the an increase in the singly oxygenated carbon peak at 286.8 eV for samples with FEC. This means surface SEI features grow as a result of electrochemistry observed in differential capacity when FEC is added to the electrolyte. This phe - nomenon follows the original hypothesis. The presence of FEC is playing a role in how the SEI is formed during the initial stages of battery as - sembly and experimentation. By studying SEI as a function of voltage the effect of FEC as perhaps a sacrificial additive can be observed more clearly. Ultimately, there is still further research needed to learn about how FEC reacts with sodium metal.

Closer examination of the newly emerged carbonate peak in the FEC MPR spectra reveals that the peak is centered around 291 eV, not 290 eV, where it is found without FEC. The disparity in binding energy of the

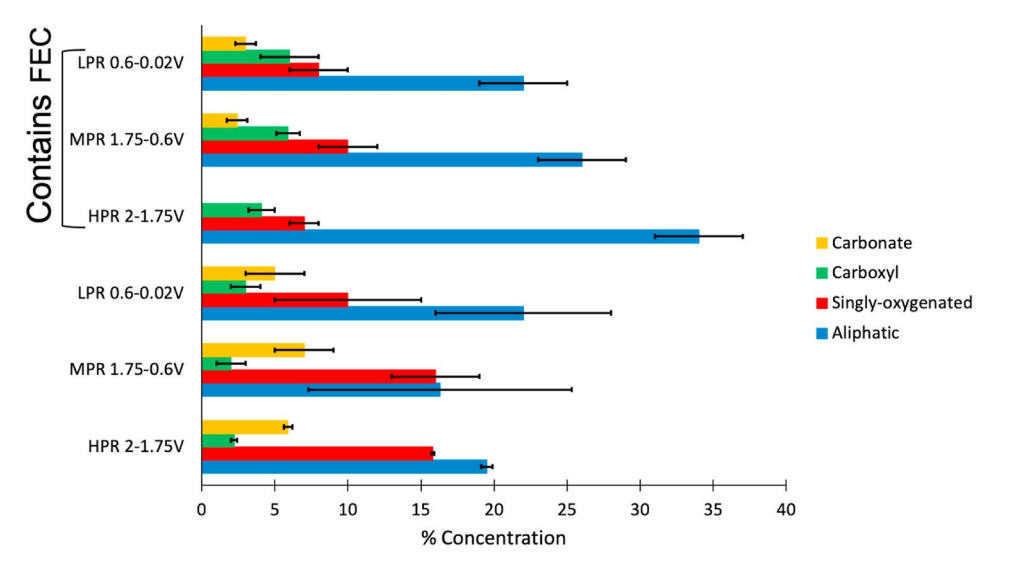
carbonate environment between the two sets of experiments is interesting as both 290 and 291 eV fit in the binding energy envelope of carbonate carbon [69]. It is unlikely the 291 eV peak in FEC experiments is fluorinated carbon, as it is commonly characterized to be, because there is no analogous fluorine peak appeared in the same XPS scan (SI figure S5), only sodium fluoride. Thus, the difference in carbonate peak position is believed to be due to the ionic carbonate environment potentially having a slightly higher binding energy than a covalent carbonate environment. Ionic carbonates form in higher concentrations when FEC is present while covalent carbonate form more commonly in samples without FEC [71].

Reviewing the LPR results, there are no new carbon environments observed, however, the singly oxygenated peak concentration, calcualted from peak area, has more error in replicate samples compared to the more oxidizing potential regions. Increased error is likely due to heterogeneities becoming exaggerated as the electrolyte is exposed to more reducing potentials. Regardless, the presence of FEC suppresses the growth of singly-oxygenated and carbonate containing components before electrochemistry has begun. Thus the organic constituents that result in the singly-oxygenated and carbonate signal in the HPR carbon XPS spectra could be a detriment to battery lifetime and can be prevented with the presence of FEC.

Oxygen 1s XPS spectra with and without FEC are shown in Fig. 5 and the corresponding quantification data reported in Fig. 6 (numerical values for average concentration and peak position present in SI table



£íg. 3. Overlaid Carbon 1s XPS spectra of all spots from replicate batteries cycled with 1 M NaClO₄ 1:1:1 EC:DMC:DEC in A) HPR, B) MPR, C) LPR without FEC and D) HPR, E) MPR, and F) LPR with FEC. Aliphatic carbon, singly oxygenated carbon, carboxyl carbon, and carbonate carbon environments are labeled at their approximate binding energy for each collection of spectra. Each overlaid spectra have an average spectra as a darker black line.



£ig. 4. Average percent concentration of carbon environments from fit XPS spectra for replicate experiments cycled with (above) and without (below) FEC in the HPR (2–1.75 V), MPR (1.75–0.6 V), and LPR (0.6–0.02 V vs. Na/Na *). Aliphatic carbon concentration is shown in blue, singly oxygenated carbon in red, carboxyl carbon in green, and carbonate carbon in yellow. (For interpretation of the references to color in this figure legend, the reader is referred to the Web version of this article.)

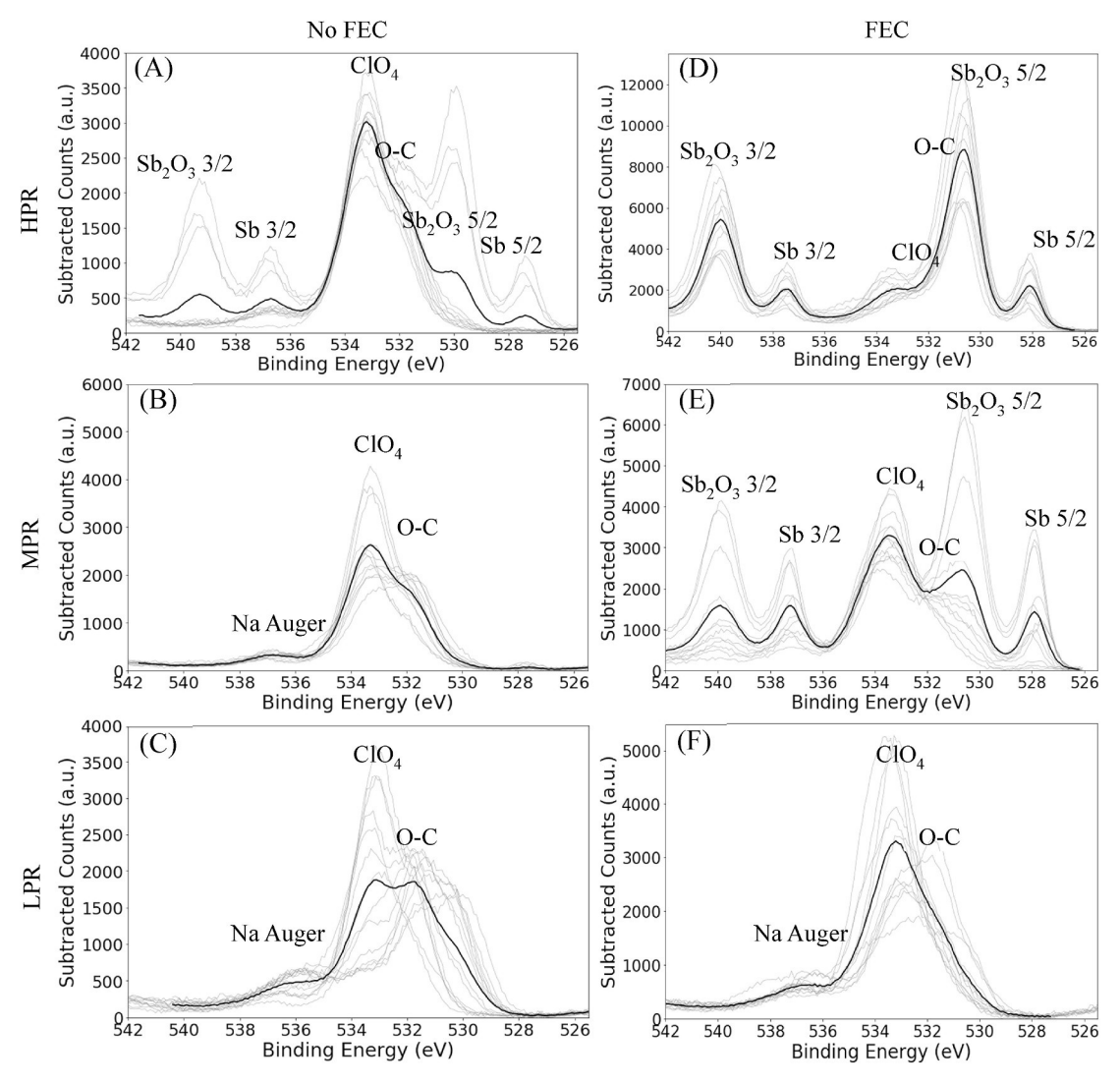


fig. 5. Overlaid oxygen 1s XPS spectra of all spots from replicate batteries cycled with 1 M NaClO₄ 1:1:1 EC:DMC:DEC in A) HPR, B) MPR, C) LPR without FEC and D) HPR, E) MPR, and F) LPR with FEC. Perchlorate oxygen, oxygen bonded to carbon, antimony and antimony oxide 3d 5/2 and 3d3/2 environments are labeled at their approximate binding energy for each collection of spectra. Each overlaid spectra have an average spectra as a darker black line.

S2). Antimony 3d photoelectron peaks appears at similar binding energies to the oxygen 1s photoelectron. Antimony has a large RSF value and, thus, is easily detected with XPS. Being a part of the electrode, if antimony is observed, the SEI is less than 10 nm thick as 10 nm is the approximate distance photoelectrons can penetrate through and be observed [69]. The antimony 3d peaks appear in the HPR and MPR FEC experiments, as well as all three spots on one sample cycled in the HPR without FEC. The presence of antimony and antimony oxide 3d 5/2 and 3d_{3/2} peaks show that the SEI in these experiments is less than 10 nm thick. The relative thickness of the samples that do not include antimony supports the results observed in the carbon spectra where samples without FEC as well as batteries cycled in the LPR have more material present in the SEI and are thus thicker.

Oxygen environments attributed to the SEI observed during these experiments include perchlorate oxygen at about 533 eV and oxygen on carbon, including any C–O and G=O species, at 531.5 eV [69,72]. These two peaks overlap in our samples, thus we did want to overinterpret the oxygen spectra so it is used as a check for when the other elements implied the presence of oxygen. Oxygen on carbon peaks are larger when FEC is not present matching carbon XPS data, while perchlorate concentrations are constant given error, the only exception being HPR FEC samples having less perchlorate oxygen than oxygen on carbon. Studying the oxygen XPS spectra in this system does not reveal the same

detail as the carbon spectra since oxygen bonded to carbon does not differentiate based upon the organic functional group in which it is contained. One final detail about the oxygen 1s spectra is when the antimony peak is obscured by the SEI, like in the no FEC MPR samples and all LPR samples, there is a small peak is present around 537 eV. This peak is the Kl_4L_{23} sodium auger peak appearing due to increased sodium concentrations in the SEI [69]. The presence of this peak further complicates fitting clear oxygen environments and drawing conclusions from the different types of oxygen that are present in the samples.

Analogous to the LPR carbon XPS spectra, replicate LPR oxygen XPS spectra were more heterogeneous than samples cycled at more oxidizing potentials. Particularly, the concentration of perchlorate oxygen fluc tuated immensely in replicate LPR experiments. Additionally, samples without FEC exhibit a new oxygen peak at 530 eV conceivably attributed to Na₂O or NaOH [69]. The sodium auger peak in the samples with no FEC in the LPR are aligned correctly showing that the peaks are calibrated correctly. These heterogeneous signals suggest that the conditions occurring on the surface when the battery is cycled in the LPR are inconsistent. The source of this inconsistency may be related to previous research showing sodium metal to be a poor reference electrode [48,49, 52–54,73]. If the reference electrode is changed, the measured voltage at the working electrode will be different than the potential it is actually experiencing. Thus it is possible that differences in the passivation of the

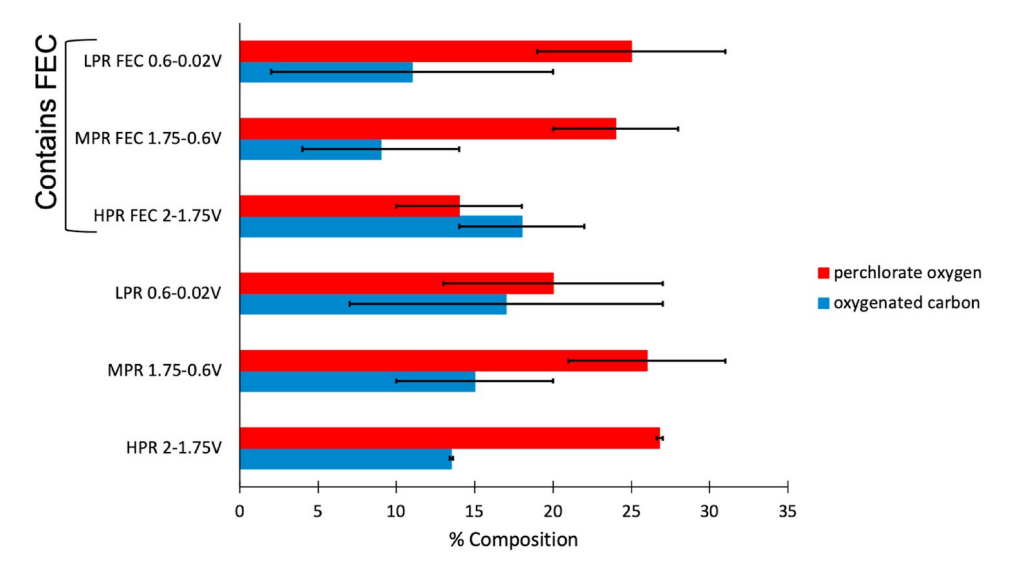


fig. 6. Average percent concentration of oxygen environments from fit XPS spectra for replicate experiments cycled with (above) and without (below) FEC in the HPR (2–1.75 V), MPR (1.75–0.6 V), and LPR (0.6–0.02 V vs. Na/Na *). Oxygenated carbon concentration is shown in blue, perchlorate oxygen in red. (For interpretation of the references to color in this figure legend, the reader is referred to the Web version of this article.)

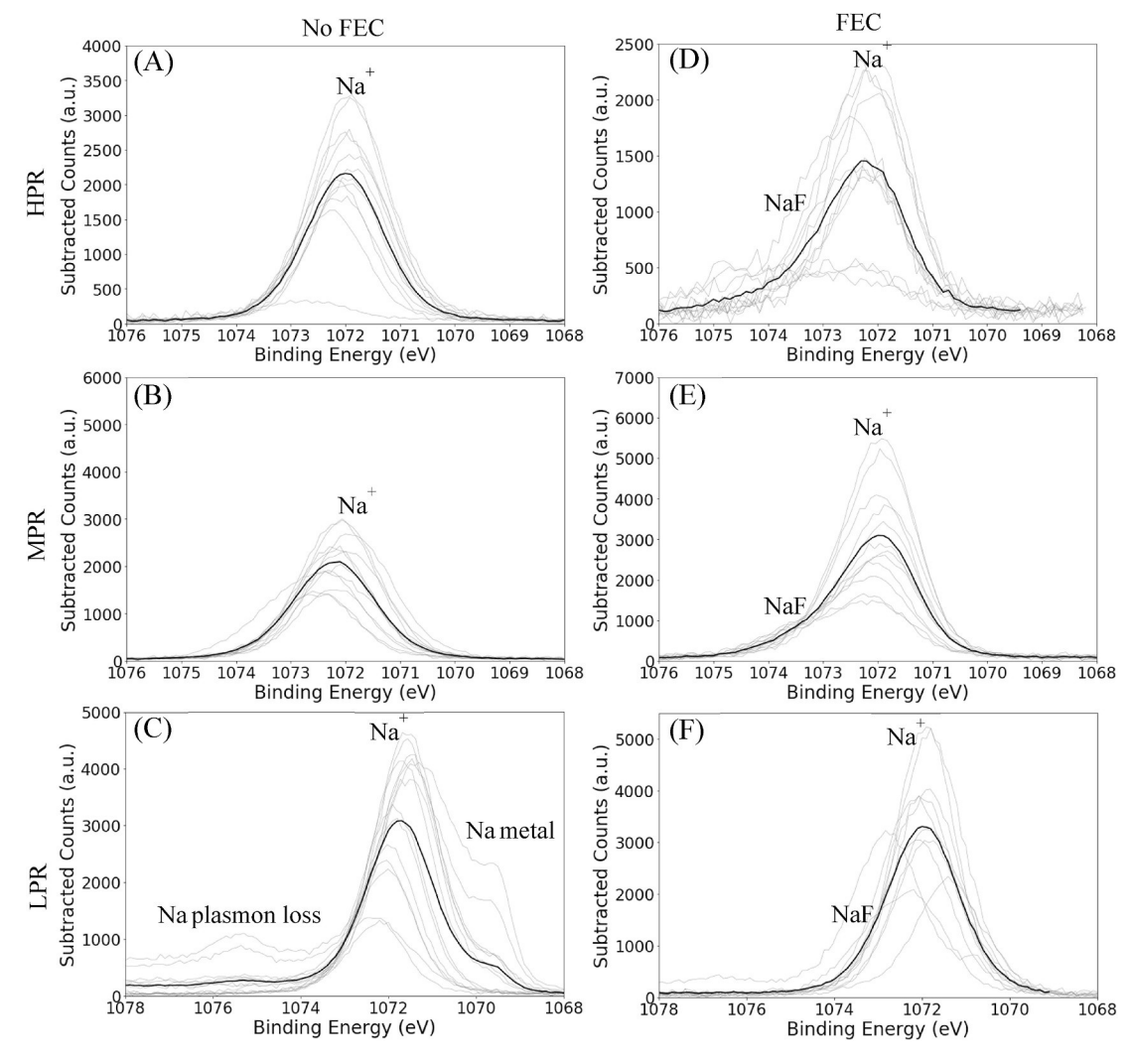


fig. 7. Overlaid sodium 1s XPS spectra of all spots from replicate batteries cycled with 1 M NaClO₄ 1:1:1 EC:DMC:DEC in A) HPR, B) MPR, C) LPR without FEC and D) HPR, E) MPR, and F) LPR with FEC. Sodium cation, sodium fluoride, and sodium metal plasmon loss environments are labeled at their approximate binding energy for each collection of spectra. Each overlaid spectra have an average spectra as a darker black line.

sodium metal pseudo-reference electrode from replicate samples compounded to the point observed in the XPS, through the different potentials felt on replicate surfaces.

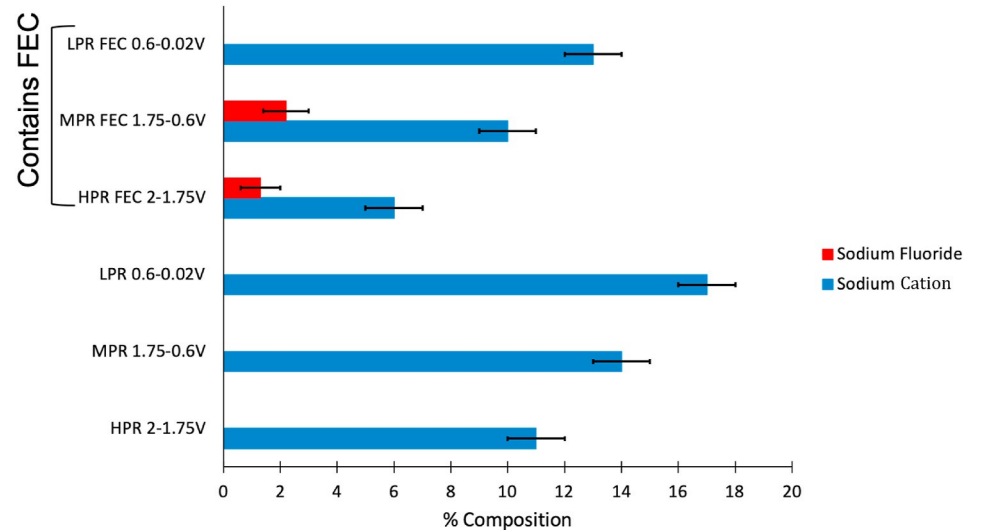
Deciphering qualitative information from the sodium 1s XPS spectra shown in Fig. 7 can be difficult as many sodium environments overlap in binding energy [69]. The general trend from the quantification data in Fig. 8 (numerical values and average peak position present in SI) reveals that on average samples without FEC contained roughly 50% higher sodium concentrations than their FEC counterparts for a given potential region. SEI reactions are likely irreversible, meaning there are signifi cant faradaic efficiency repercussions for supporting electrolyte consumption. Sodium concentrations also increase as batteries are cycled at more reducing potentials, reflecting the increase in the KL $_{1}L_{23}$ sodium auger peak observed in the oxygen 1s spectra. Sodium plays an important role in the SEI makeup as it is the only cation in the system. This means any anion formed from the electrolyte decomposition couples with sodium, and, if insoluble, precipitates onto the surface as part of the SEI. The primary peak at 1072 eV is likely comprised of Na₂CO₃, NaClO₄, and other larger carbon anions such as NaROCO [69]. The primary sodium peak at 1072 eV does not move in position across every sample collected. Additionally, samples containing FEC have a shoulder at higher binding energies centered at 1073.5 eV due to the presence of NaF that is known to have a different binding energy than other sodium salts [69]. Examining the Na 1s XPS spectra of FEC containing batteries cycled in the LPR reveals certain scans show the shoulder peak to be more intense than the primary peak. This level of heterogeneity lead to quantification results that could not be compared directly and were thus omitted. The reason for this heterogeneity is likely the same for the differences observed in the oxygen XPS spectra, relating to inconsistent passivation of the sodium counter electrode inducing irreproducible potentials on the surface of Cu₂Sb when cycled in LPR conditions.

The LPR Na spectra without FEC displayed different features on certain scans which is not present in any HPR or MPR experiments. Complimentary peaks at 1075 eV and 1070 eV appear together and were not quantified. These peaks are thought to be due to plasmon loss of sodium metal, which has not been heavily documented in literature due to the extremely reactive surface that is quickly oxidized to form sodium salts. This phenomenon would not have been observed without the capability to perform XPS experiments air-free. Plasmon loss is not observed on pristine sodium metal surface as prepared for half-cell ex -periments (SI Figure S7). However, this feature has been observed before supporting the conclusion that sodium metal is present, heteroge -neously, across LPR samples without FEC [74,75]. The presence of sodium metal as shown from the plasmon feature in certain LPR samples

supports the hypothesis that the potential on the surface is not accu rately between 0.6 and 0.02 V vs. Na/Na + (an expanded plot of the sodium plasmon effect as well as the auger peaks are shown in SI Figure S8). The reaction of sodium metal with the electrolyte passivated the sodium counter electrode to the extent that instead of holding a 0.02 V vs Na/Na +, the working electrode felt a voltage below the 0 V vs Na/Na⁺ plating the observed sodium metal on the surface. The previous research on sodium metal half cells has shown sodium to be a non-ideal pseudo-reference and the presence of plasmon peak may be an artifact of sodium counter electrode being overly altered [48,49,52,53,73]. An alternative hypothesis for this observation is that the SEI in the sample with no FEC in the LPR became too thick, thereby developing a signif icant overpotential resulting in sodium metal plating. However, the cycling program did not allow for the voltage to go below 0 V vs. Na/Na⁺, and we observe no signature of Na plating in the dQ/dV plots. Despite these potentially variable conditions, the presence of FEC leads to the formation of NaF, which may also play a role in how FEC expands battery lifetime although XPS is incapable of explaining why. Never theless, XPS has shown significantly differing results based upon the presence of FEC and has revealed the extent to which the initial discharge affects SEI formation in sodium half-cell batteries on elec trodeposited Cu₂Sb.

4. Conclusion

XPS was used to study the SEI formed on electrodeposited Cu 2Sb half-cell anodes in a sodium system using conventional electrolytes with and without the presence of the FEC small molecule additive, previously observed to dramatically extend battery lifetime. Specifically, the initial discharge of these batteries was broken into potential regions based on the electrochemistry occurring in differential capacity plots in order to probe the SEI formation. Initially, it was thought that electrochemistry observed in differential capacity could be correlated to chemical envi ronments in XPS. However, in samples cycled without FEC singly oxygenated and carbonate carbon appeared in the HPR where little to no electrochemistry was observed in the corresponding differential capac ity plot contradicting the hypothesis. Alternatively, in samples containing FEC a carbonate peak appeared in the MPR samples after electrochemistry was observed in the differential capacity supporting the hypothesis. Additionally, studying replicate experiments revealed how the heterogeneity manifested itself at more reducing potentials. Ultimately, the system is more complicated than scope of the original hypothesis as it is likely the sodium metal pseudo-reference counter electrode is responsible for the different results observed. The HPR



£ig. 8. Average percent concentration of sodium cation environments from fit XPS spectra for replicate experiments cycled with (above) and without (below) FEC in the HPR (2–1.75 V), MPR (1.75–0.6 V), and LPR (0.6–0.02 V vs. Na/Na ⁺). The primary sodium cation concentration is shown in blue, sodium fluoride in red. Note, so dium fluoride was present in LPR samples with FEC but heterogeneity prevented an accurate quantification. (For interpretation of the references to color in this figure legend, the reader is referred to the Web version of this article.)

samples without FEC show significant SEI formation without considerable electrochemistry occurring, suggesting spontaneous electrolyte reactivity had occurred. Our hypothesis is that the products of the re action between conventional electrolyte and sodium metal deposit on the surface of the pure phase Cu₂Sb active material as an SEI. The additive FEC may be creating a protective layer on sodium metal through its own spontaneous reaction to prevent other electrolyte reactions instead of sacrificially electrochemically reducing onto the anode's surface. This hypothesis goes against previous work with FEC in the lithium system and implies that the identity of the anode material may not necessarily play a significant role in SEI formation, but the use of sodium in a half cell is a very important consideration. Additionally, the complicating effect of the sodium counter electrode was observed at more reducing potentials as its unreliability as a reference electrode resulted in electroplated sodium metal on the working electrode. Determining the extent of the effect of this reactivity is the focus of ongoing research especially in relation to FEC. Additionally, examina tion of any electrolyte reactivity for sodium ion batteries, should be explored in full cell battery experiments. These results show that FEC is able to passivate sodium metal differently than the conventional elec trolytes, which has significant impact on how the SEI grows on the anode material and the function of the additive in sodium ion systems. This report has highlighted the importance for understanding electrolyte-surface interaction during the initial discharge of a half cell experiment and demonstrated the importance of FEC in that first interaction. Furthermore, the results have broad implications in the development of new sodium ion battery materials and electrolytes, the creation of a fast ion conductors, or a sodium metal anode battery

CRedit authorship contribution statement

Mathan J. Gimble: Formal analysis, Data curation, Writing - original draftWriting - original draft, Writing - review & editingWriting - review & editing, was responsible for the battery cycling and XPS experiments, formal data analysis, data curation, and writing the initial drafts as well as the reviewing and editing of the manuscript. Leslie A. Kraynak: Conceptualization, Methodology, is responsible for conceptualization and methodology as well as assisting with the initial depositions of Cu2Sb and data interpretation of the XPS obtained on these samples. Jacob D. Schneiber: Writing - original draftWriting - original draft, designed and built the air-free sample holder used to obtain the XPS data described in this manuscript. Maxwell C. Schulze: Software, Writing original draftWriting - original draft, Formal analysis, is responsible for the software used in the manuscript that assisted with data analysis. Amy L. Prieto: Project administration, Funding acquisition, Resources, Writing - original draftWriting - original draft, is behind project administration and obtaining the funding and resources for this work as well as assisted with the design of experiments and editing the manu script. The use of additives changes for the formation of the SEI on binderless, dense anodes in Na-ion batteries.

Declaration of competing interest

The authors have no competing interest to declare.

Acknowledgements

This work was funded by the United State National Science Foun dation Solid State and Materials Chemistry program - 1710672. Special thanks to the Central Instrument Facility staff at Colorado State University, especially Dr. Patrick McCurdy for his help with XPS.

Appendix A. Supplementary data

Supplementary data to this article can be found online at https://doi.

org/10.1016/j.jpowsour.2020.229171.

References

- [1] J.A. Church, N.J. White, A 20th century acceleration in global sea-level rise, Geophys. Res. Lett. 33 (2006), https://doi.org/10.1029/2005GL024826, 2018.
- [2] D. Larcher, J.M. Tarascon, Towards greener and more sustainable batteries for electrical energy storage, Nat. Chem. 7 (2015) 19–29, https://doi.org/10.1038/ nchem.2085.
- [3] K. Xu, Electrolytes and interphases in Li-ion batteries and beyond, Chem. Rev. 114 (2014) 11503–11618, https://doi.org/10.1021/cr500003w.
- [4] J.B. Goodenough, Energy storage materials: a perspective, Energy Storage Mater 1 (2015) 158–161, https://doi.org/10.1016/j.ensm.2015.07.001.
- [5] M.R. Palacin, A. de Guibert, Why do batteries fail? Science 351 (80) (2016) https://doi.org/10.1126/science.1253292, 1253292–1253292.
- [6] S.S. Zhang, A review on electrolyte additives for lithium-ion batteries, J. Power Sources 162 (2006) 1379–1394, https://doi.org/10.1016/j.jpowsour.2006.07.074.
- [7] D. Aurbach, Y. Ein-Eli, B. Markovsky, A. Zaban, S. Luski, Y. Carmeli, H. Yamin, The study of electrolyte solutions based on ethylene and diethyl carbonates for rechargeable Li batteries, J. Electrochem. Soc. 142 (1995) 2882–2890, https://doi. org/10.1149/1.2048659.
- [8] E.B.Y. Radarweg, N.X. Amsterdam, E.B. All, U.S. Government, S. Batteries, L.R. Systems, O. The, C.H. Applications, E. Vehicles, F.C. The, A. Weber, F. Cells, S. Oxide, L.C. The, W.S. Fuels, H. Production, N. Gas, S.S.R. The, M.D.F. Production, G. Cleaning, M.S. The, K. Bullock, L. Systems, P. Acid, I. No, From: Encyclopedia of Electrochemical Power Sources, vol. 3. Elsevier. Amsterdam, 2009, p. 2009.
- [9] T. Richard, J.K. Xu, O. Borodin, M. Ue, Modern Aspects of Electrochemistry, vol. 58, n.d, http://www.springer.com/series/6251 (accessed October 25, 2019).
- [10] A.M. Haregewoin, A.S. Wotango, B.-J. Hwang, R.L. Sacci, T.M. Fears, Y. Wang, J. F. Browning, S. Thevuthasan, D.R. Baer, C.-M. Wang, L. Zhang, F. Kang, Electrolyte additives for lithium ion battery electrodes: progress and perspectives, Energy Environ, Sci. 9 (2016) 1955–1988. https://doi.org/10.1039/C6EE.00123h
- [11] C.L. Campion, W. Li, B.L. Lucht, Thermal decomposition of LiPF 6 -based electrolytes for lithium-ion batteries, J. Electrochem. Soc. 152 (2005) A2327–A2334. https://doi.org/10.1149/1.2083267
- [12] G.G. Eshetu, T. Diemant, M. Hekmatfar, S. Grugeon, R.J. Behm, S. Laruelle, M. Armand, S. Passerini, Impact of the electrolyte salt anion on the solid electrolyte interphase formation in sodium ion batteries, Nanomater. Energy 55 (2019) 327–340, https://doi.org/10.1016/j.nanoen.2018.10.040.
- [13] C. Ge, L. Wang, L. Xue, Z.-S. Wu, H. Li, Z. Gong, X.-D. Zhang, Synthesis of novel organic-ligand-doped sodium bis(oxalate)-borate complexes with tailored thermal stability and enhanced ion conductivity for sodium ion batteries, J. Power Sources 248 (2014) 77–82, https://doi.org/10.1016/j.jpowsour.2013.09.044.
- [14] A. Ponrouch, E. Marchante, M. Courty, J.-M. Tarascon, M.R. Palacín, P. Poizot, J.-M. Tarascon, C. Delmas, K. Fujiwara, In search of an optimized electrolyte for Naion batteries, Energy Environ. Sci. 5 (2012) 8572, https://doi.org/10.1039/ 020223288b
- [15] S.J. An, J. Li, C. Daniel, D. Mohanty, S. Nagpure, D.L. Wood, The state of understanding of the lithium-ion-battery graphite solid electrolyte interphase (SEI) and its relationship to formation cycling, Carbon N. Y. 105 (2016) 52–76, https:// doi.org/10.1016/j.carbon.2016.04.008.
- [16] F.A. Soto, A. Marzouk, F. El-Mellouhi, P.B. Balbuena, Understanding ionic diffusion through SEI components for lithium-ion and sodium-ion batteries: insights from first-principles calculations, Chem. Mater. (2018), https://doi.org/10.1021/acs. chemmater.8b00635 acs.chemmater.8b00635.
- [17] M. Lu, H. Cheng, Y. Yang, A comparison of solid electrolyte interphase (SEI) on the artificial graphite anode of the aged and cycled commercial lithium ion cells, Electrochim. Acta 53 (2008) 3539–3546, https://doi.org/10.1016/j. electrochim. 2007.09.062
- [18] E. Peled, S. Menkin, Review—SEI: past, present and future, J. Electrochem. Soc. 164 (2017) A1703–A1719, https://doi.org/10.1149/2.1441707jes.
- [19] P. Verma, P. Maire, P. Novák, A review of the features and analyses of the solid electrolyte interphase in Li-ion batteries, Electrochim. Acta 55 (2010) 6332–6341, https://doi.org/10.1016/J.ELECTACTA.2010.05.072.
- [20] Y. Matsumura, S. Wang, J. Mondori, Mechanism leading to irreversible capacity loss in Li ion rechargeable batteries, J. Electrochem. Soc. 142 (1995) 2914, https://doi.org/10.1149/1.2048665.
- [21] J.B. Goodenough, K.-S. Park, The Li-ion rechargeable battery: a perspective, J. Am. Chem. Soc. 135 (2013) 1167–1176, https://doi.org/10.1021/ja3091438.
- [22] P. Arora, R.E. White, M. Doyle, Capacity fade mechanisms and side reactions in lithium-ion batteries, J. Electrochem. Soc. 145 (1998) 3647, https://doi.org/ 10.1149/1.1838857
- [23] D. Aurbach, K. Gamolsky, B. Markovsky, Y. Gofer, M. Schmidt, U. Heider, On the use of vinylene carbonate (VC) as an additive to electrolyte solutions for Li-ion batteries, Electrochim. Acta 47 (2002) 1423–1439, https://doi.org/10.1016/ S0013-4686(01)00858-1.
- [24] H. Ota, Y. Sakata, A. Inoue, S. Yamaguchi, Analysis of vinylene carbonate derived SEI layers on graphite anode, J. Electrochem. Soc. 151 (2004) A1659, https://doi. org/10.1149/1.1785795
- [25] I.A. Shkrob, J.F. Wishart, D.P. Abraham, What makes fluoroethylene carbonate different? J. Phys. Chem. C (2015) https://doi.org/10.1021/acs.jpcc.5b03591.
- [26] E.D. Jackson, A.L. Prieto, Copper antimonide nanowire array lithium ion anodes stabilized by electrolyte additives, ACS Appl. Mater. Interfaces 8 (2016) 30379–30386, https://doi.org/10.1021/acsami.6b08033.

- [27] K. Schroder, J. Alvarado, T.A. Yersak, J. Li, N. Dudney, L.J. Webb, Y.S. Meng, K. J. Stevenson, The effect of fluoroethylene carbonate as an additive on the solid electrolyte interphase on silicon lithium-ion electrodes, Chem. Mater. 27 (2015) 5531–5542, https://doi.org/10.1021/acs.chemmater.5b01627.
- [28] V. Etacheri, O. Haik, Y. Goffer, G.A. Roberts, I.C. Stefan, R. Fasching, D. Aurbach, Effect of fluoroethylene carbonate (FEC) on the performance and surface chemistry of Si-nanowire Li-ion battery anodes, Langmuir 28 (2012) 965–976, https://doi. org/10.1021/la203712s.
- [29] H. Nakai, T. Kubota, A. Kita, A. Kawashima, Investigation of the solid electrolyte interphase formed by fluoroethylene carbonate on Si electrodes, J. Electrochem. Soc. 158 (2011) A798, https://doi.org/10.1149/1.3589300.
- [30] J.M. Martínez de la Hoz, P.B. Balbuena, Reduction mechanisms of additives on Si anodes of Li-ion batteries, Phys. Chem. Chem. Phys. 16 (2014) 17091–17098, https://doi.org/10.1039/c4cp01948b.
- [31] A.L. Michan, B.S. Parimalam, M. Leskes, R.N. Kerber, T. Yoon, C.P. Grey, B. L. Lucht, Fluoroethylene carbonate and vinylene carbonate reduction: understanding lithium-ion battery electrolyte additives and solid electrolyte interphase formation, Chem. Mater. 28 (2016) 8149–8159, https://doi.org/10.1021/acs.chemmater.6b02282.
- [32] Y. Jin, N.-J.H.J.H. Kneusels, P.C.M. Magusin, G. Kim, E. Castillo-Martínez, L. E. Marbella, R.N. Kerber, D.J. Howe, S. Paul, T. Liu, C.P. Grey, Identifying the structural basis for the increased stability of the solid electrolyte interphase formed on silicon with the additive fluoroethylene carbonate, J. Am. Chem. Soc. 139 (2017) 14992–15004, https://doi.org/10.1021/jacs.7b06834.
- [33] K. Leung, S.B. Rempe, M.E. Foster, Y. Ma, J.M. Martinez del la Hoz, N. Sai, P. B. Balbuena, Modeling electrochemical decomposition of fluoroethylene carbonate on silicon anode surfaces in lithium ion batteries, J. Electrochem. Soc. 161 (2013) A213–A221, https://doi.org/10.1149/2.092401jes.
- [34] R. Jung, M. Metzger, D. Haering, S. Solchenbach, C. Marino, N. Tsiouvaras, C. Stinner, H.A. Gasteiger, Consumption of fluoroethylene carbonate (FEC) on Si-C composite electrodes for Li-ion batteries, J. Electrochem. Soc. (2016), https://doi. org/10.1149/2.0951608jes.
- [35] C. Xu, F. Lindgren, B. Philippe, M. Gorgoi, F. Bjorefors, K. Edstrom, T. Gustafsson, Improved performance of the silicon anode for Li-ion batteries: understanding the surface modification mechanism of fluoroethylene carbonate as an effective electrolyte additive, Chem. Mater. 27 (2015) 2591–2599, https://doi.org/ 10.1021/acs.chemmater.5b00339.
- [36] Y. Jin, N.J.H. Kneusels, L.E. Marbella, E. Castillo-Martinez, P.C.M.M. Magusin, R. S. Weatherup, E. Jonsson, T. Liu, S. Paul, C.P. Grey, Understanding fluoroethylene carbonate and vinylene carbonate based electrolytes for Si anodes in lithium ion batteries with NMR spectroscopy, J. Am. Chem. Soc. (2018), https://doi.org/10.1021/jacs.8b03408.
- [37] A. Bouibes, N. Takenaka, T. Fujie, K. Kubota, S. Komaba, M. Nagaoka, Concentration Effect of Fluoroethylene Carbonate on the Formation of Solid Electrolyte Interphase Layer in Sodium-Ion Batteries, 2018, https://doi.org/ 10.1021/acsami.8b07530.
- [38] S. Komaba, T. Ishikawa, N. Yabuuchi, W. Murata, A. Ito, Y. Ohsawa, Fluorinated ethylene carbonate as electrolyte additive for rechargeable Na batteries, ACS Appl. Mater. Interfaces 3 (2011) 4165–4168. https://doi.org/10.1021/am200973k.
- [39] M. Dahbi, T. Nakano, N. Yabuuchi, S. Fujimura, K. Chihara, K. Kubota, J.-Y. Son, Y.-T. Cui, H. Oji, S. Komaba, Effect of hexafluorophosphate and fluoroethylene carbonate on electrochemical performance and the surface layer of hard carbon for sodium-ion batteries, ChemElectroChem 3 (2016) 1856–1867, https://doi.org/10.1002/celc.201600365.
- [40] M. Gauthier, T.J. Carney, A. Grimaud, L. Giordano, N. Pour, H.H. Chang, D. P. Fenning, S.F. Lux, O. Paschos, C. Bauer, F. Maglia, S. Lupart, P. Lamp, Y. Shao-Horn, Electrode-electrolyte interface in Li-ion batteries: current understanding and new insights, J. Phys. Chem. Lett. 6 (2015) 4653–4672, https://doi.org/10.1021/acs.joclett.5b01727.
- [41] A. Tokranov, R. Kumar, C. Li, S. Minne, X. Xiao, B.W. Sheldon, Control and optimization of the electrochemical and mechanical properties of the solid electrolyte interphase on silicon electrodes in lithium ion batteries, Adv. Energy Mater. 6 (2016) 1502302, https://doi.org/10.1002/aenm.201502302.
- [42] Z. Liu, P. Lu, Q. Zhang, X. Xiao, Y. Qi, L.Q. Chen, A bottom-up formation mechanism of solid electrolyte interphase revealed by isotope-assisted time-offlight secondary ion mass spectrometry, J. Phys. Chem. Lett. 9 (2018) 5508–5514, https://doi.org/10.1021/acs.jpclett.8b02350.
- [43] B. Key, R. Bhattacharyya, M. Morcrette, V. Sezréc, J.-M. Tarascon, C.P. Grey, Real-time NMR investigations of structural changes in silicon electrodes for lithium-ion batteries, J. Am. Chem. Soc. 131 (2009) 9239–9249, https://doi.org/10.1021/isp096278
- [44] O. Borodin, X. Ren, J. Vatamanu, A. von Wald Cresce, J. Knap, K. Xu, Modeling insight into battery electrolyte electrochemical stability and interfacial structure, Acc. Chem. Res. 50 (2017) 2886–2894, https://doi.org/10.1021/acs. accounts.7b00486.
- [45] A. Wang, S. Kadam, H. Li, S. Shi, Y. Qi, Review on modeling of the anode solid electrolyte interphase (SEI) for lithium-ion batteries, Npj Comput. Mater. 4 (2018) 15, https://doi.org/10.1038/s41524-018-0064-0.
- [46] S.-W. Kim, D.-H. Seo, X. Ma, G. Ceder, K. Kang, Electrode materials for rechargeable sodium-ion batteries: potential alternatives to current lithium-ion batteries, Adv. Energy Mater. 2 (2012) 710–721, https://doi.org/10.1002/ aenm.201200026.
- [47] S.P. Ong, V.L. Chevrier, G. Hautier, A. Jain, C. Moore, S. Kim, X. Ma, G. Ceder, Voltage, stability and diffusion barrier differences between sodium-ion and lithium-ion intercalation materials, Energy Environ. Sci. 4 (2011) 3680, https:// doi.org/10.1039/c1ee01782a.

- [48] D.I. Iermakova, R. Dugas, M.R. Palacín, A. Ponrouch, On the comparative stability of Li and Na metal anode interfaces in conventional alkyl carbonate electrolytes, J. Electrochem. Soc. 162 (2015) A7060–A7066, https://doi.org/10.1149/ 2.0001513ias
- [49] R. Dugas, A. Ponrouch, G. Gachot, R. David, M.R. Palacin, J.M. Tarascon, Na reactivity toward carbonate-based electrolytes: the effect of FEC as additive, J. Electrochem. Soc. 163 (2016) A2333–A2339, https://doi.org/10.1149/ 2.0981610jae
- [50] K. Pfeifer, S. Arnold, J. Becherer, C. Das, J. Maibach, H. Ehrenberg, S. Dsoke, Can metallic sodium electrodes affect the electrochemistry of sodium-ion batteries? Reactivity issues and perspectives, ChemSusChem 12 (2019), https://doi.org/ 10.1002/cssc.201901056 cssc.201901056.
- [51] M. Zarrabeitia, M. Á. Munoz-Márquez, F. Nobili, T. Rojo, M. Casas-Cabanas, Influence of using metallic na on the interfacial and transport properties of Na-Ion batteries, Batteries 3 (2017) 16, https://doi.org/10.3390/batteries3020016.
- [52] S.E. Lee, M.H. Tang, Reliable reference electrodes for nonaqueous sodium-ion batteries, J. Electrochem. Soc. 166 (2019) A3260–A3264, https://doi.org/ 10.1149/2.0401914jes
- [53] A. Boschin, M.E. Abdelhamid, P. Johansson, On the feasibility of sodium metal as pseudo-reference electrode in solid state electrochemical cells, ChemElectroChem 4 (2017) 2717–2721, https://doi.org/10.1002/celc.201700273.
- [54] S.E. Lee, M.H. Tang, Electroactive decomposition products cause erroneous intercalation signals in sodium-ion batteries, Electrochem. Commun. 100 (2019) 70–73, https://doi.org/10.1016/j.elecom.2019.01.024.
- [55] V. Winkler, G. Kilibarda, S. Schlabach, D.V. Szab, T. Hanemann, M. Bruns, Surface analytical study regarding the solid electrolyte interphase composition of nanoparticulate SnO2 anodes for Li-ion batteries, J. Phys. Chem. C 120 (2016) 24706–24714, https://doi.org/10.1021/acs.jpcc.6b06662.
- [56] B. Philippe, M. Hahlin, K. Edstrom, T. Gustafsson, H. Siegbahn, H. Rensmo, Photoelectron spectroscopy for lithium battery interface studies, J. Electrochem. Soc. 163 (2016) A178–A191, https://doi.org/10.1149/2.0051602jes.
- [57] M.J. Zachman, Z. Tu, S. Choudhury, L.A. Archer, L.F. Kourkoutis, Cryo-STEM mapping of solid–liquid interfaces and dendrites in lithium-metal batteries, Nature 560 (2018) 345–349, https://doi.org/10.1038/s41586-018-0397-3.
- [58] C. Bommier, X. Ji, Electrolytes, SEI formation, and binders: a review of nonelectrode factors for sodium-ion battery anodes, Small 14 (2018) 1703576, https://doi.org/10.1002/smll.201703576.
- [59] L. Baggetto, P. Ganesh, R.P. Meisner, R.R. Unocic, J.-C. Jumas, C.A. Bridges, G. M. Veith, Characterization of sodium ion electrochemical reaction with tin anodes: experiment and theory, J. Power Sources 234 (2013) 48–59, https://doi.org/10.1016/j.joowsour.2013.01.083.
- [60] L. Bodenes, A. Darwiche, L. Monconduit, H. Martinez, The Solid Electrolyte Interphase a key parameter of the high performance of Sb in sodium-ion batteries: comparative X-ray Photoelectron Spectroscopy study of Sb/Na-ion and Sb/Li-ion batteries, J. Power Sources 273 (2015) 14–24, https://doi.org/10.1016/j. ipowsour_2014_09_037.
- [61] A. Darwiche, L. Bodenes, L. Madec, L. Monconduit, H. Martinez, Impact of the salts and solvents on the SEI formation in Sb/Na batteries: an XPS analysis, Electrochim. Acta 207 (2016) 284–292, https://doi.org/10.1016/j.electacta.2016.03.089.
- [62] P. Lu, C. Li, E.W. Schneider, S.J. Harris, Chemistry, impedance, and morphology evolution in solid electrolyte interphase films during formation in lithium ion batteries, J. Phys. Chem. C 118 (2013) 896–903, https://doi.org/10.1021/ ip4111019
- [63] L. Baggetto, E. Allcorn, A. Manthiram, G.M. Veith, Cu2Sb thin films as anode for Na-ion batteries, Electrochem. Commun. 27 (2013) 168–171, https://doi.org/ 10.1016/j.elecom.2012.11.030.
- [64] L.M.L. Fransson, J.T. Vaughey, R. Benedek, K. Edstrom, J.O. Thomas, M. M. Thackeray, Phase Transitions in Lithiated Cu2Sb Anodes for Lithium Batteries: an in Situ X-Ray Diffraction Study, 2001, https://doi.org/10.1016/S1388-2481 (01)00140-0
- [65] M.M. Thackeray, J.T. Vaughey, C.S. Johnson, A.J. Kropf, R. Benedek, L.M. L. Fransson, K. Edstrom, Structural considerations of intermetallic electrodes for lithium batteries, J. Power Sources 113 (2003) 124–130, https://doi.org/10.1016/ S0378-7753(02)00538-4.
- [66] J.M. Mosby, A.L. Prieto, Direct electrodeposition of Cu2Sb for lithium-ion battery anodes, J. Am. Chem. Soc. 130 (2008) 10656–10661, https://doi.org/10.1021/ ion02/1658
- [67] S. Evans, Correction for the effects of adventitious carbon overlayers in quantitative XPS analysis, Surf. Interface Anal. 25 (1997) 924–930, https://doi. org/10.1002/(SICI)1096-9918(199711)25:12 <924::AID-SIA317>3.0.CO;2-2.
- [68] G. Greczynski, L. Hultman, X-ray photoelectron spectroscopy: towards reliable binding energy referencing, Prog. Mater. Sci. 107 (2020), https://doi.org/ 10.1016/j.pmatsci.2019.100591.
- [69] J.F. Moulder, W.F. Stickle, P.E. Sobol, K.D. Bomben, Handbook of X-Ray Photoelectron Spectroscopy, vol. 55344, Physical Electronics, Inc., Eden Prairie, Minesota, 1992.
- [70] M.C. Schulze, R.K. Schulze, A.L. Prieto, Electrodeposited thin-film CuXSb anodes for Li-ion batteries: enhancement of cycle life via tuning of film composition and engineering of the film-substrate interface, J. Mater. Chem. A. 6 (2018) 12708–12717, https://doi.org/10.1039/c8ta01798k.
- [71] R. Dedryvère, L. Gireaud, S. Grugeon, S. Laruelle, J.-M. Tarascon, D. Gonbeau, Characterization of Lithium Alkyl Carbonates by X-Ray Photoelectron Spectroscopy: Experimental and Theoretical Study, 2005, https://doi.org/ 10.1021/JP051626K.
- [72] B.C. Beard, Fresh cleaved single crystal NaCl, XPS spectra, Al source, Surf. Sci. Spectra 2 (1993) 91–96, https://doi.org/10.1116/1.1247741.

- [73] J. Conder, C. Villevieille, How reliable is the Na metal as a counter electrode in Naion half cells? Chem. Commun. 55 (2019) 1275–1278, https://doi.org/10.1039/ C8CC07852A
- [74] A. Barrie, F.J.J. Street, An Auger' and X-Ray Photoelectron Spectroscopic Study of Sodium Metal and Sodium Oxide, Elsevier, 1975, https://doi.org/10.1016/0368-2048(75)80052-1.
- [75] S.P. Kowalczyk, L. Ley, F.R. McFeely, R.A. Pollak, D.A. Shirley, X-ray photoemission from sodium and lithium, Phys. Rev. B 8 (1973) 3583–3585, https://doi.org/10.1103/PhysRevB.8.3583.